PERGAMON

Continental Shelf Research 22 (2002) 1795–1810

CONTINENTAL SHELF RESEARCH

www.elsevier.com/locate/csr

Intermediate modelling of tidal inlet systems: spatial asymmetries in flow and mean sediment transport

S.M. van Leeuwen*, H.E. de Swart

Institute for Marine and Atmospheric research Utrecht, Utrecht University, Princetonplein 5, 3508 TA, Utrecht, Netherlands

Received 28 November 2000; accepted 3 December 2001

Abstract

In order to identify mechanisms which determine the morphology of tidal inlet systems, experiments with a shallow water model and sediment transport model of intermediate complexity are carried out and interpreted. A highly schematised geometry is used, consisting of a rectangular outer area connected to a rectangular basin by a narrow strait. The bottom topography is either flat or constantly sloping in the landward direction and the bed is composed of fine sand. Forcing at the open boundary consists of prescribed water levels, which can represent a (shore-parallel) progressive tidal wave or a fully standing wave. The symmetry breaking effects of Coriolis force and a progressive Kelvin wave on the tidal motion, the mean flow field and the mean sediment transport field are investigated. Tidal ellipticity properties on the outer delta are also discussed. Experiments for a rectangular basin without outer area are carried out in order to compare the intermediate model results with those of a 1D idealised model. The overall agreement is satisfactory. Next the influence of earth rotation and of the progressive wave in the outer sea on mean sediment transport in the basin is investigated. It turns out that both effects, which cannot be included in the idealised model, lead to different patterns of erosion and deposition. In both sets of experiments the effects of a progressive Kelvin wave were found to be dominant over earth rotation effects in the flow and mean sediment transport fields.

Keywords: Tidal basin; Tidal ellipticity; Residual flow; Sediment transport; Wadden Sea

1. Introduction

Tidal inlets are found along many coasts, including the east coast of North America and the Wadden Sea area (North-West Europe). A tidal inlet system consists of an inner basin which is connected to the outer sea by a narrow strait between two barrier islands. Its shallow seaward extension is called the outer delta. Most of these systems are characterised by moderate to strong tides (compared to wave effects) a complex bathymetry (channels and shoals) and residual circulation cells (see e.g. FitzGerald, 1996 and references herein). Quasi-realistic models have demonstrated that the tidal hydrodynamics (Ridderinkhof, 1988; see also Ridderinkhof and Zimmerman, 1992) and the morphologic evolution (cf. Wang et al., 1995; Cayocca, 2001) of such systems (over periods of several years) can be simulated rather well. However, due to their

*Corresponding author. Fax: +31-30-254-3163.
E-mail address: s.m.vanleeuwen@phys.uu.nl (S.M. van Leeuwen).

0278-4343/02/$ - see front matter
PII: S0278-4343(02)00038-9

complexity it is difficult to gain fundamental knowledge from such models. Alternatively, idealised models have been analysed for the tidal motion (Friedrichs and Aubrey, 1994; Lanzoni and Seminara, 1998) and the morphology (Schuttelaars and De Swart, 1999; Van Leeuwen et al., 2000) in sheltered embayments. A problem with these models is that they cannot easily be extended to more realistic tidal inlet systems. The general aim of the present study is to provide a link between quasi-realistic models and idealised semi-analytical models. This is done by carrying out experiments with a numerical model for the water motion, which is supplemented with a simple sediment transport routine, using simplified geometries. The model is, therefore, referred to as an intermediate model.

The focus of this work is on properties of tidal motion, mean flow and sediment transport. The motivation for this choice is that both tidal asymmetry and residual currents induce mean transport of sediment (Van de Kreeke and Robaczewska, 1993; Van der Molen, 2000), whilst knowledge about the latter is important to understand bathymetric changes. Field data and model studies of Dutch Wadden Sea basins indicate that tidal current characteristics and residual circulations have an asymmetrical pattern. Fig. 1(a) shows the observed tidal ellipses on the outer delta and in the strait of the Marsdiep, the most southern inlet in the Wadden Sea. Clearly, the tide is more elliptical on the northern side than on the southern side. Fig. 1(b) shows the presence of residual eddies near the Vlie inlet. It can be seen that both the sizes and the strength of the circulations vary considerably.

According to Sha (1989) the asymmetry of tidal properties on the outer delta is due to the interaction between the shore-parallel tidal currents and the currents in the strait. Then this degree of asymmetry should change if the characteristics of the tidal wave in the outer sea changes from a progressive to a more standing character. This item is relevant because along the east coast of the United States much smaller tidal phase variations occur than in the Wadden Sea. But there is also another source of symmetry breaking: the Coriolis force. Therefore, in this paper the separate and combined symmetry breaking effects of earth rotation and of a shore-parallel tidal wave on the hydro- and morphodynamics are investigated. Using a highly schematised inlet system, distinction can be made between these effects and other (topographical) influences.

Furthermore, the intermediate model is used to test results obtained previously with an idealised model (Schuttelaars and De Swart, 1996) which also includes sediment transport. If the solution of

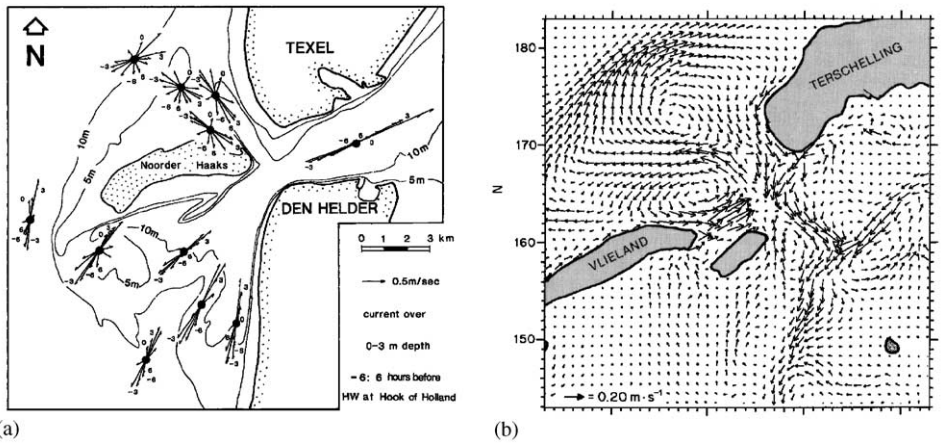

Fig. 1. Results from previous studies: (a) observed tidal ellipses in the Marsdiep inlet (from Sha, 1989); (b) numerical model results from Ridderinkhof (1988), showing residual circulation cells near the Vlie inlet. Both tidal inlets are located in the western part of the Wadden Sea.

the idealised model is also found by the intermediate model, extensions can be added and investigated which could not be included in the idealised model. Specific items in this respect are the effect of earth rotation and that of a progressive tidal wave on mean sediment transport and the relative contributions of advective and diffusive processes to the tidally averaged sediment flux.

2. The model

The numerical model HAMSOM (HAMburg Shelf Ocean Model) is used to compute the water motion. This model is based on the shallow water equations (see Appendix A), for details see Backhaus (1983). Here only the one-layer version is used. An adjustment has been made to include linear bottom friction next to quadratic bottom friction. This is relevant for comparison with the idealised model results. The HAMSOM code has also been extended with a module which describes the suspended load transport of fine sand (grain size of order 2×10^{-4} m). This formulation explicitly accounts for the effect of settling lags. The characteristic deposition timescale is of the order of a few minutes.

2.1. Geometry

The geometry represents a highly schematised tidal inlet system consisting of an inner basin which is connected through a narrow inlet to the adjacent sea. Lengths, widths and depths can be varied. Fig. 2 shows the default geometry and the bottom profiles used in this paper. The values are representative for a typical Wadden Sea inlet system (the Frisian Inlet system, see Oost, 1995). With a maximum M_2 amplitude of 1.5 m, the minimum depth is kept at 2 m below the undisturbed water level to avoid drying and flooding of banks. Hypsometric effects are, therefore, not included in these experiments.

The model is forced by prescribed free surface elevations at the open boundaries (the dashed lines in Fig. 2). Only M_2 forcing has been applied. The nature of the tidal wave can be varied from

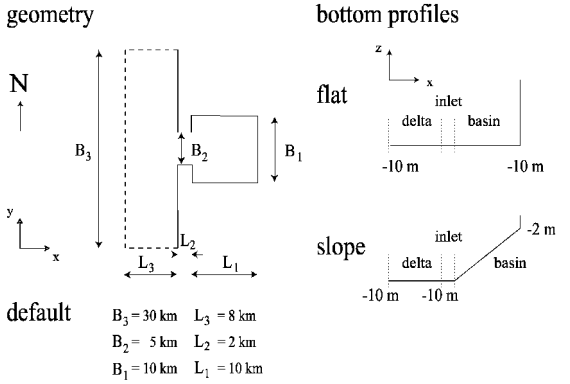

Fig. 2. The geometry and depth profiles used in the extended HAMSOM model simulations. Top view (left) and depth profiles along central axis (right). The dashed lines in the top view plot represent open boundaries where free surface elevations are prescribed.

travelling to a full standing wave and the typical friction timescale is of the order of one day. The default set-up includes a grid-size of $\sim$400 m in the x-direction (landward direction, west to east) and $\sim$600 m in the y-direction (along-shore direction, south to north) and a time step of 60 s. Simulations were always done for a period of 3 weeks with output only on the last four days. The default case further includes a horizontal diffusion coefficient for the water motion of $10\,\mathrm{m^2\,s^{-1}}$. Due to the difference in research aims concerning the tidal flow field (outer area characteristics) and mean sediment transport (comparison to idealised model), different default geometries, bottom friction parameterisation and tidal amplitudes were used.

2.2. Sediment transport formulation

To account for sediment transport the HAMSOM model was extended with a sediment transport module. The concentration of suspended sediment is determined by

$$\frac{\partial C}{\partial t}+\vec{\nabla}\cdot(\vec{u}C-\mu\vec{\nabla}C)=\alpha(\vec{u}^2)-\gamma C. \qquad (1)$$

Eq. (1) is the conservation equation for the *depth-integrated* concentration C. The time evolution of the amount of sediment in the water column is determined by advective and diffusive transport of

the sediment and by deposition of sediment on the bed or erosion of it from the bed. The parameters and variables used are: $\vec{u} = (u, v)$ the depth-averaged velocity vector, consisting of the cross-shore (u) and along-shore (v) velocity components, $\mu \sim 50\,\mathrm{m^2 s^{-1}}$ a horizontal diffusion coefficient, $\alpha \sim 10^{-2}\,\mathrm{kg\,s\,m^{-4}}$ an erosion coefficient and $\gamma \sim 4 \times 10^{-3}\,\mathrm{s^{-1}}$ a deposition coefficient. For more information on this parameterisation see Dyer (1986) and Van Rijn (1993). The values are representative for the Frisian Inlet system (Oost, 1995; Schuttelaars and De Swart, 1996). The critical velocity for erosion is set to zero. It is assumed that the depth-averaged velocity exceeds the critical depth-averaged erosion velocity for the larger part of the tidal cycle.

The settling time scale $2\pi/\gamma$ is of the order of a few minutes, whereas the time scale of the water motion is the tidal period $2\pi/\sigma$. The ratio of the settling time scale over the tidal period is the parameter $a = \sigma/\gamma \sim 10^{-2}$. An approximate solution to Eq. (1) can be found by a perturbation method, using the fact that a is a small parameter. In zeroth order this leads to a balance between erosion and deposition near the bed, which determines the depth-integrated concentration given by C_0. The first-order correction to C_0 is also used and is given by C_1

$$C_0 = \frac{\alpha}{\gamma}\vec{u}^2, \quad C_1 = -\frac{1}{\gamma}\left\{\frac{\partial C_0}{\partial t} + \vec{\nabla}\cdot(\vec{u}C_0)\right\}. \tag{2}$$

The depth-integrated concentration implemented in the sediment module is therefore $C = C_0 + C_1$. The sediment flux $\vec{F}$ is determined by Eq. (3) and accounts for both diffusive and advective sediment transport

$$\vec{F} = \vec{F}_{adv} + \vec{F}_{diff} = \vec{u}C - \mu\vec{\nabla}C. \tag{3}$$

Divergence and convergence of the sediment flux will determine locations of erosion and deposition, respectively.

3. Residual circulation patterns and tidal characteristics

Experiments were carried out to investigate whether the present model is able to simulate similar tidal characteristics as those obtained by Ridderinkhof (1988) and those discussed in Sha (1989). This means that the effects of earth rotation and a Kelvin wave passing the inlet entrance on the water motion (including the tidally averaged circulation) are investigated. The default case represents a standing wave in the outer sea and excludes the effects of earth rotation. The standing wave forcing without Coriolis effects is not the situation found in the Wadden Sea system, but was chosen as a reference case to investigate the separate symmetry breaking effects of the progressive wave following the coast and the effects induced by earth rotation. The strength of the progressive wave is determined by the imposed phase difference between the southern and northern boundary and denoted by the time difference Δt. This time difference is defined as the time that it takes for high water to reach the northern open boundary, starting at the southern open boundary. The progressive wave represents a Kelvin wave which on the Northern Hemisphere always travels with the coast on the right-hand side. Quadratic bottom friction and an M_2 amplitude of 1.5 m are used. Results are shown for the default geometry with a sloping bottom (see Fig. 2).

3.1. Tidal asymmetry on the outer delta

First, we consider to what extent the conceptual model of Sha (1989) is confirmed by the results of the present model. Sha's model attributes the asymmetry in the morphology and tidal current characteristics in the outer area to the interaction of the shore-parallel tidal current and the current in the strait. In Fig. 3, current ellipses are shown for the default situation (i.e., a standing tidal wave is forced in the outer sea), next with Coriolis effects included (Fig. 3(b)) and finally for the case of default settings but with forcing by a progressive tidal wave (Fig. 3(c)). This wave is travelling from south (bottom of picture) to north (top of picture) and has a time lag over the open boundary of 3000 s in Fig. 3(c). Note that 3000 s is the maximum time lag allowed and represents the time needed by a propagating Kelvin wave to travel 30 km. A decrease in the amplitude due to friction is not incorporated in the boundary conditions.

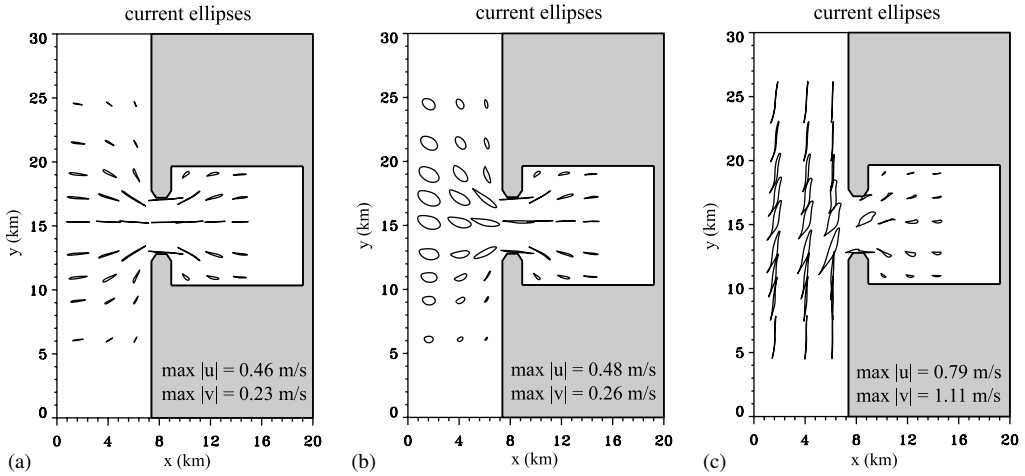

Fig. 3. Current ellipses for a sloping bottom in the inner basin and (a) default case, (b) default case with Coriolis effects and (c) default case with tidal wave travelling from south to north, time lag between southern and northern boundary $\Delta t = 3000$ s. Direction of rotation is (a) clockwise, (b) clockwise, (c) anti-clockwise. Grey area is land.

This is because the frictional length scale of the progressive wave is much longer than the length of the western (seaward) open boundary.

As can be seen from Fig. 3(b) earth rotation causes both an increase in tidal ellipticity and spatial differences in the orientation of the tidal ellipses over the outer area, compared with the default situation. A strong decrease in tidal ellipticity on the outer delta is observed (Fig. 3(c)) if the Kelvin wave is imposed. The latter forcing induces much stronger flood and ebb velocities, causing the tidal ellipses to become more bi-directional. The combined effect of earth rotation and a progressive Kelvin wave yields the same result as in Fig. 3(c). A clear difference in ellipticity between the northern and southern part of the outer area is not found, except in a very small region attached to the northern headland (not visible here). The polarisation of the tidal current in Figs. 3(a) and (b) is clockwise, whilst in Fig. 3(c) (representative for Wadden Sea basins) it is anti-clockwise. Sha (1989) found clockwise polarisation of tidal currents (Fig. 1(a)) from data of the Marsdiep inlet in the Dutch Wadden Sea. The difference with the model result of Fig. 3(c) may be attributed to the fact that the Marsdiep inlet has a much larger basin length than that of the basin considered in our experiments. Consequently, tidal characteristics in both inlet systems are different, e.g. in the Marsdiep basin the tidal amplitude increases towards the land due to resonance behaviour. Also the presence of a large shoal on the outer delta of the Marsdiep inlet may affect the polarisation of the tidal current.

The velocity fields during maximum ebb and maximum flood in the strait for the case of the progressive tidal wave are shown in Fig. 4. As can be seen in Fig. 4(b), an overshoot of the flood current when entering the embayment was not found in runs with the present geometry. When the strait is made very narrow (~ 1 km) and the described forcings are maintained an overshoot of the flood current is found, but this is not a realistic situation for the inlets in the Dutch Wadden Sea. Thus, the present results do not fully support the conceptual ideas introduced by Sha (1989).

3.2. Mean flow field

The tidally averaged flow field is shown for the default case (Fig. 5(a)), the default case with Coriolis effects (Fig. 5(b)) and for the default case

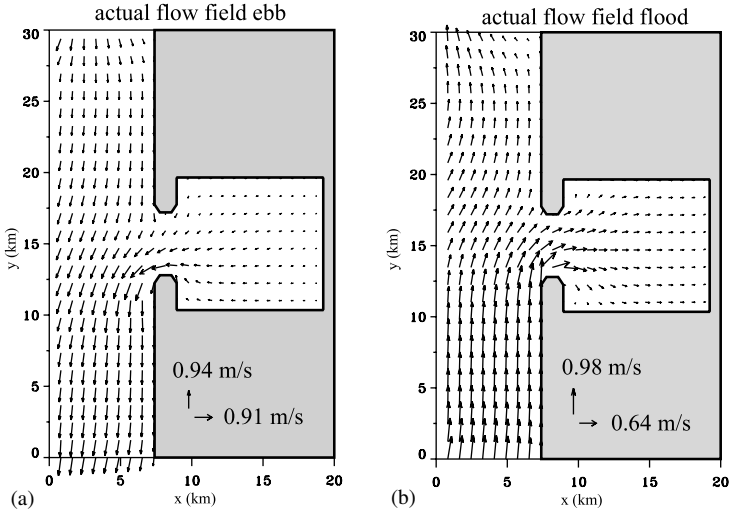

Fig. 4. Flow field at maximum ebb (a) and maximum flood (b) for a sloping bottom in the inner basin. Default case with combined effects of Coriolis and a tidal wave travelling from south to north, time lag between southern and northern boundary $\Delta t = 3000$ s. Grey area is land.

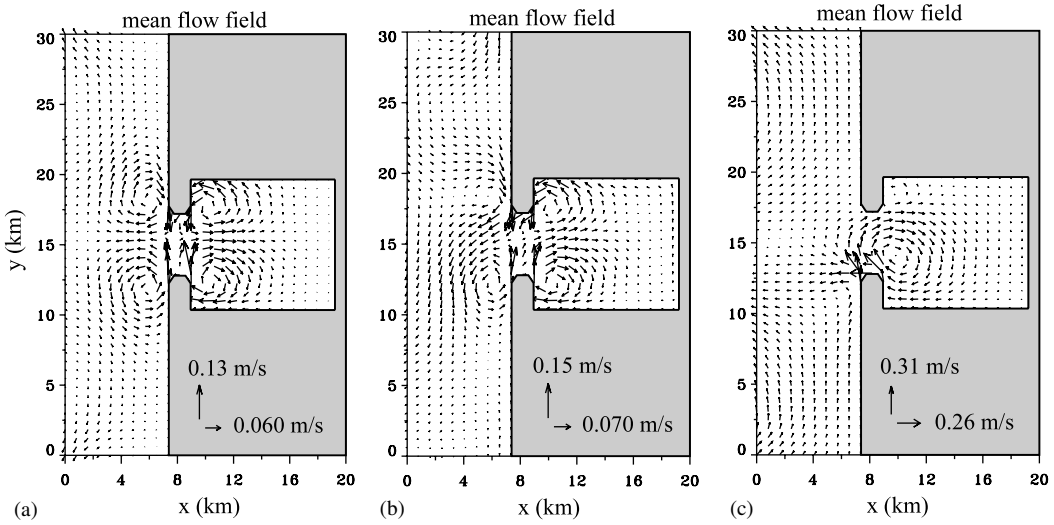

Fig. 5. Mean flow field results for a sloping bottom in the inner basin and (a) default case (no Coriolis force, time lag $\Delta t = 0$ s), (b) default case with Coriolis force and (c) default case with a tidal wave travelling from south (bottom of picture) to north (top of picture), time lag between southern and northern boundary $\Delta t = 3000$ s. Grey area is land, the arrows below the basin show the absolute maximum velocity in each direction.

with a progressive Kelvin wave with a time lag over the open boundary of 3000 s (Fig. 5(c)).

Without the Coriolis force and with forcing by a standing tidal wave four identical residual circulation cells around the inlet are found. These cells are the result of tidal rectification induced by frictional boundary layers near the sidewalls and they are referred to as *headland eddie*s. The

mechanism can be described as follows. During the flood stage (defined here as $u > 0$ in the strait) positive (negative) tidal vorticity is generated at the northern (southern) side of the inlet and transported by tidal currents into the basin. During the ebb stage negative (positive) vorticity is produced on the northern (southern) side of the inlet and advected to the outer sea. This results in the quadrupole pattern of Fig. 5(a). For more details about the underlying physics see Zimmerman (1981).

When the Coriolis force is included the joint action of earth rotation and bottom friction causes an oblique orientation of the tidal ellipses with respect to the central axis (see Fig. 3(b)). Also the orientation of the ellipses changes over the outer area between south and north. Process analysis revealed that in this case additional vorticity (besides the vorticity discussed above) is generated in the outer sea due to cross-shore shear of the longshore velocity component (i.e., $\partial v/\partial x$). Consider the situation during flood and distinguish between two stages: one during which $v > 0$ at the southern side of the outer sea and one during which $v < 0$ at the northern side. Then during the first flood stage negative vorticity, generated at the southern side of the outer area, is imported into the basin. During the second flood stage import takes place of additional positive vorticity which is produced at the northern side. The asymmetrical distribution of the tidal current properties and vorticity production over the outer area results in a net transport of negative vorticity into the basin. During ebb the same mechanism causes a net additional export of positive vorticity towards the outer area. This explains why in Fig. 5(b) the southern (northern) residual circulation cells in both the outer area and in the basin are strengthened (weakened) when they are compared with those shown in Fig. 5(a). The production of vorticity by the Coriolis force itself is not large enough to be important here. Bottom frictional torques due to the sloping bottom were also found to be of minor importance: the same results were obtained for a flat bottom topography.

If a weak phase difference over the open boundary is imposed (time lag $\Delta t = 1500$ s, not shown here) and earth rotation excluded, the mean flow field is dominated by a large southern basin cell and a smaller northern basin cell. A strong phase difference over the open boundary ($\Delta t = 3000$ s, Fig. 5(c)) results in an even more dominant southern basin cell and a disappearing northern one. In the outer area a remnant of the southern cell can still be seen. The flow in the seaward part is now too strong for the cells in the outer delta to develop (compare the maximum velocities in Figs. 5(b) and (c)). The pattern shown in Fig. 5(c) can be understood as follows. As the flow in the outer area now has a travelling wave character the shore-parallel tidal current and the current in the strait have a phase difference. Process analysis showed that also in this case the governing mechanism is related to the generation of tidal velocity shear due to sidewall friction. Still the mechanism resulting in the headland eddies of Fig. 5(a) is active. Since the first part of flood is now much longer in duration than the second part of flood, the result is a stronger net import of negative vorticity than in the previous case. This causes the negative residual circulation cell inside the basin to be strengthened while the positive one is weakened. Again, the same results were found for a flat bottom topography, indicating the minor importance of bottom frictional torques here.

Including both Coriolis and the progressive tidal wave results in the same pattern as in Fig. 5(c). Thus, the model results seem to indicate that in systems like the Western Dutch Wadden Sea the Kelvin wave following the coast has a much stronger symmetry breaking effect than the Coriolis force. However, they do not explain the residual flow pattern shown in Fig. 1(b). This is because the residual circulation cells in the Wadden Sea are largely the result of tidal rectification related to bottom frictional torques induced by a laterally sloping bottom (Ridderinkhof, 1988).

3.3. Mean sea level

Fig. 6 shows the mean sea level for the three cases presented above.

In the default case a symmetrical pattern around the inlet axis is found, consisting of a set-up in the basin and in the northern and southern part of the

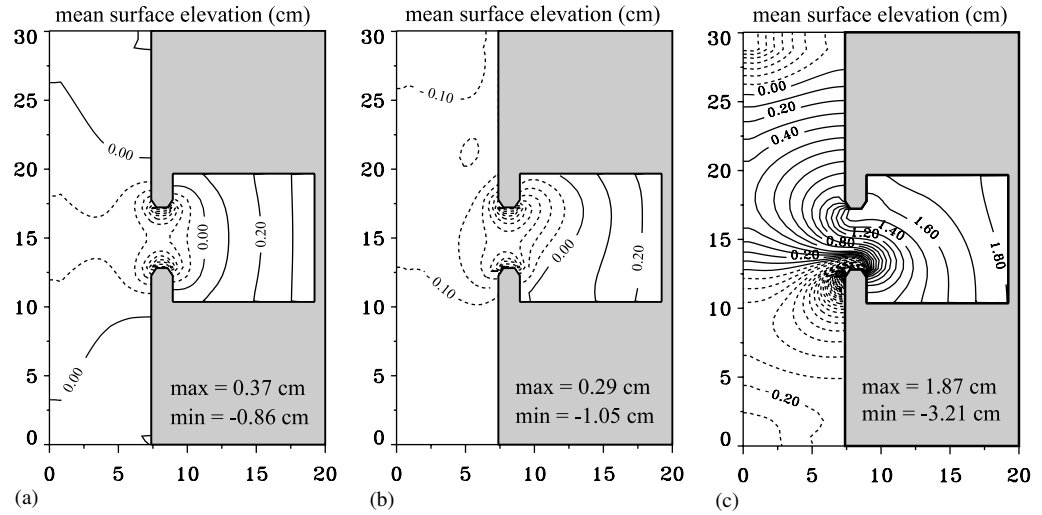

Fig. 6. Mean surface elevation results for a sloping bottom in the inner basin and (a) default case, (b) default case with Coriolis and (c) with progressive tidal wave travelling from south to north, time lag between southern and northern boundary $\Delta t = 3000$ s. Contour lines are drawn for each 0.1 cm, dashed lines represent negative surface elevation. The thicker solid line is the zero line. Grey area is land.

outer area and a set-down in the inlet. A mean sea level set-down in the inlet and set-up in the basin were also found by Ridderinkhof (1988) and are considered to be general features in inlet systems. They can be understood from Bernoulli's principle: as the flow accelerates and decelerates along a streamline during both entering and exiting the inlet, the divergence of tidal stress is balanced by the water-level gradient. This gradient will be negative when entering the inlet and positive when exiting the inlet (because velocities are larger in the strait than in the outer area and basin), causing a set-down over the inlet in the direction of the flow. In the cross-inlet direction the set-down at the headlands is the result of the balance between centrifugal acceleration and the water-level gradient (Ridderinkhof, 1988).

With only Coriolis force to break the symmetry, a stronger set-down is found near the northern headland than near the southern headland (Fig. 6(b)). In the cross-inlet direction the balance is now between centrifugal acceleration, Coriolis acceleration and the water-level gradient (Ridderinkhof, 1988). As the first of these does not change sign between ebb and flood (as the Coriolis acceleration does), the water-level gradient will be stronger during flood (negative gradient) than during ebb (positive gradient), resulting in a stronger mean water-level minimum on the side of the northern headland.

The progressive tidal wave generates a higher set-up at the end of the basin as well as a set-up in the northern part of the outer delta (Fig. 6(c)). This increase in mean water-level values is strongly dependent upon the imposed phase difference: in case of the progressive wave with $\Delta t = 1500$ s the maximum set-up is 0.97 cm and the maximum set-down -1.82 cm. The results shown here indicate a strong dependence on the phase difference imposed on the open boundary of the outer delta. Thus, the influence of the time lag of the tidal wave travelling along the shore on the mean sea surface level is much larger than that of earth rotation effects.

4. Mean sediment transport

In the second series of experiments the emphasis is on tidally averaged sediment transport. It will

be studied whether the present numerical model confirms the earlier obtained results of 1D idealised models (Schuttelaars and De Swart, 1996, 1999). The latter suggest that sediment transport in a basin tends to zero if the depth decreases in the landward direction with a constant slope. The idealised models also assume that, if there is no connecting strait, then at the transition embayment-sea a zero divergence of the net sediment flux occurs.

To check and extend these findings with the present model, the geometry is simplified to a rectangular embayment (see Fig. 2, with $L_2 = L_3 = 0\,\text{km}$, $L_1 = 20\,\text{km}$ and $B_2 = 10\,\text{km}$). The default case now includes a uniform M_2 amplitude of 1.5 m at the open boundary and linear bottom friction, in accordance with the formulations used in the idealised model. Results are discussed for a horizontal flat bed and for a sloping bottom profile (Fig. 2).

4.1. Comparison with 1D idealised results

Fig. 7 shows the advective and diffusive sediment flux (see Eq. (3)) along the central axis of the embayment computed with the intermediate model and the idealised model for both a horizontal bottom and a constantly sloping bottom. The fluxes have been scaled with their maximum values.

The profiles of the mean fluxes calculated with the two models show good comparison. The maximum values of the mean fluxes are shown in Table 1.

In case of a flat bottom the magnitudes of the fluxes agree as well. However, the results from the intermediate model show an increase in mean sediment transports in the case of a sloping topography, whilst in the idealised model sediment fluxes decrease when the bottom approaches the equilibrium profile (the constantly sloping bottom $h = x$ in which the separate sediment fluxes become zero). This is because in the idealised model a degenerated version of the momentum equations is solved, in which the effect of bottom friction is ignored. The latter causes additional phase differences between velocity and concentration (apart from those generated by settling lag effects) and thus induces additional mean sediment transport. Thus, the present intermediate model results indicate that bottom friction should be accounted for when computing mean sediment transport.

The resemblance between the models appears to hold as long as the forcing is not too strong (causing larger water-level set-up, larger velocity values) and as long as no partial drying and flooding of shoals occurs. Since the latter process is essential to reach morphodynamic equilibrium in the idealised models, the conclusion is that the intermediate model is not yet suitable for simulating morphodynamic equilibria. However, it can be used to study the influence of physical processes that cannot be incorporated in the idealised model in the non-equilibrium conditions considered in this paper.

4.2. Effect of earth rotation

The influence of earth rotation on the mean flow field and mean sediment transport is investigated by slowly increasing the Coriolis parameter f. Results are shown in Fig. 8 for 30° North and 52° North. Without Coriolis a symmetrical outflow of water and inflow of sediment is found. The HAMSOM model allows for a Stokes drift into

Table 1

	Flat bottom			Sloping bottom		
	$\bar{F}_{adv}$ (kg/ms)	$\bar{F}_{diff}$ (kg/ms)	$\frac{\bar{F}_{adv}}{\bar{F}_{diff}}$ (kg/ms)	$\bar{F}_{adv}$ (kg/ms)	$\bar{F}_{diff}$ (kg/ms)	$\frac{\bar{F}_{adv}}{\bar{F}_{diff}}$ (kg/ms)
Intermediate model	1.45 E−5	2.08 E−4	0.070	6.08 E−5	2.33 E−4	0.26
Idealised model	2.25 E−5	4.11 E−4	0.055	7.60 E−6	3.81 E−4	0.020

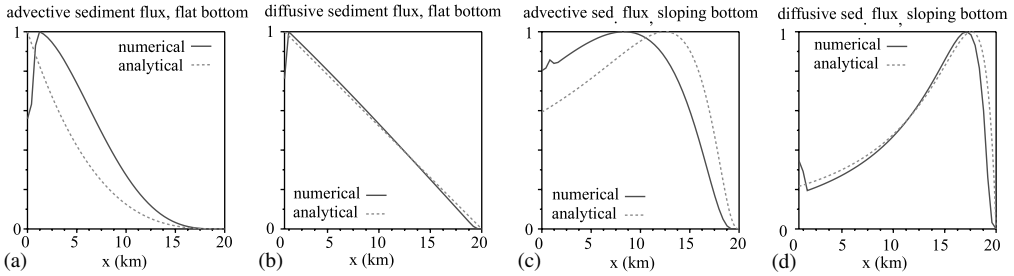

Fig. 7. Profiles of tidally averaged fluxes along the central axis of the basin, computed with the 1D analytical model and with the intermediate numerical model: (a) advective sediment flux, horizontal bottom; (b) diffusive sediment flux, horizontal bottom; (c) advective sediment flux, sloping bottom and (d) diffusive sediment flux, sloping bottom.

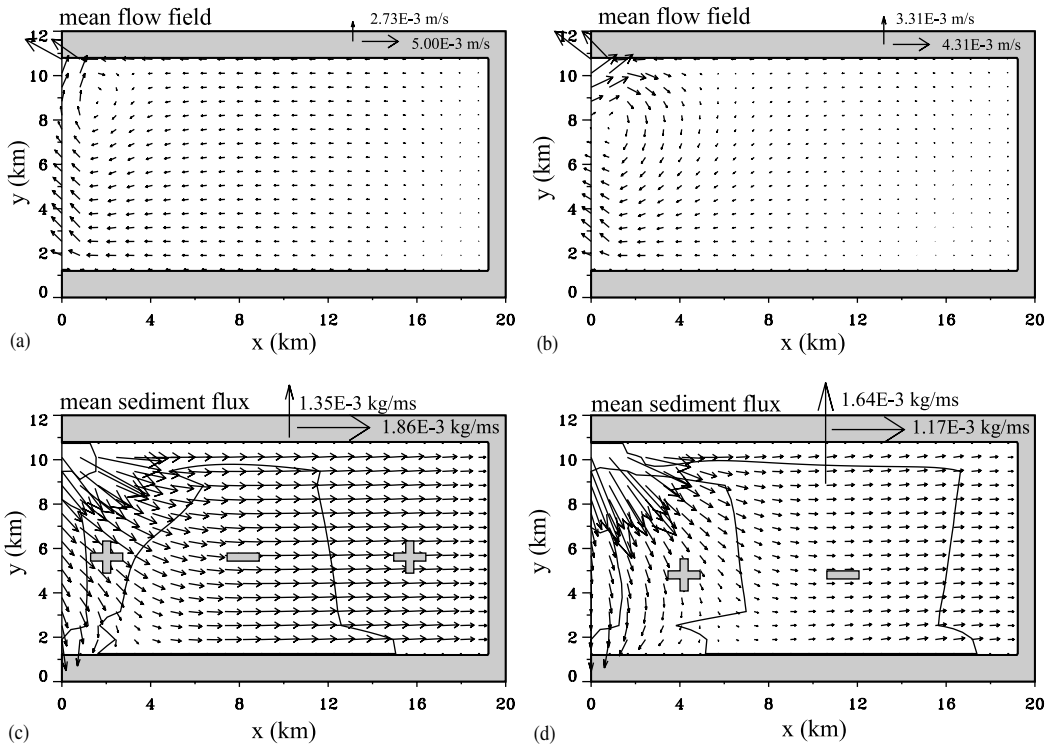

Fig. 8. Mean flow field (top) and mean sediment flux field (bottom) for default settings and Coriolis: (a, c) 30° North; (b, d) 52° North. The drawn line is zero convergence of sediment flux, the grey signs indicate deposition (plus) and erosion (minus) areas.

the basin (due to frictional effects), which results in a small outward directed mean flow component.

Fig. 8 shows that with increasing Coriolis a residual cell with anti-cyclonic rotation occurs in the inlet entrance. Its presence is clear for f values representing latitudes of 20° and more. The same pattern was found for a flat bottom topography. The presence of this residual circulation cell

appears to be a consequence of the imposed boundary condition at the entrance (prescribed water level without cross-channel variation). For non-zero values of f this induces a cross-channel velocity component at this location of which the amplitude increases with f. In combination with the presence of along-channel water depth gradients a bottom frictional torque occurs at the entrance. Process analysis revealed that this frictional torque dominates over the one induced by planetary vortex stretching. The result is that during flood negative vorticity is produced which is transported into the basin. During ebb, positive vorticity is produced which is transported out of the basin, causing a net build up of negative vorticity in the basin. The length of the cell is determined by the tidal excursion length, which can be estimated at $UT \sim 6$ km. A sloping bottom enhances the strength of the cell since the current, deflected by earth rotation, experiences a cross-current slope. The residual circulation cell is, therefore, a result of the imposed boundary condition, but can also be interpreted as the result of an outside source of negative vorticity during flood, e.g. caused by outer delta topography.

The tidally averaged sediment transport is inward directed (purely landward directed for $f = 0$) and curves to the right as Coriolis increases. Figs. 8(c) and (d) show a convergence of the sediment flux near the seaward and landward boundary of the embayment, resulting in deposition of sediment in those areas. The erosion in the central area is weaker and extends further into the basin as Coriolis effects become smaller. At the same time, the magnitude of the sediment fluxes decreases. This is mainly due to the decrease of the advective flux in the landward direction, caused by the decrease in the landward-directed velocity.

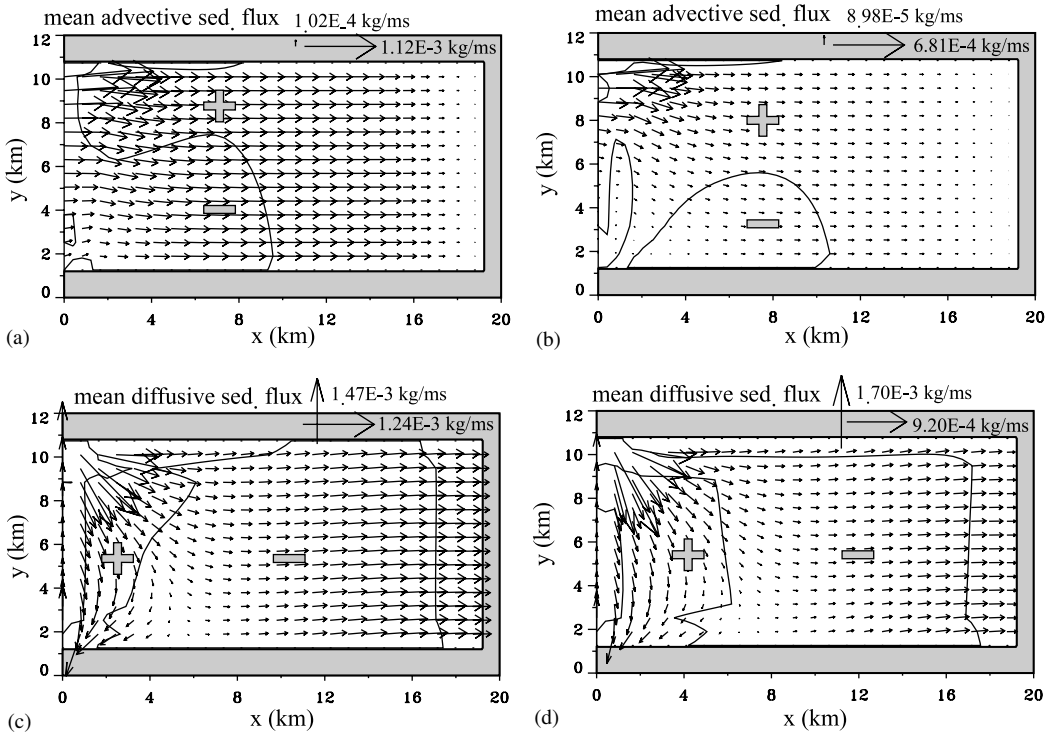

Fig. 9. Mean advective sediment flux field (top) and mean diffusive sediment flux field (bottom) for default settings and Coriolis: (a, c) 30° North; (b, d) 52° North. The drawn line is zero convergence of the plotted sediment flux, the grey signs indicate deposition (plus) and erosion (minus) areas.

Fig. 9 shows the advective and diffusive (see Eq. (3)) mean sediment transport patterns for the two cases. Fig. 9(a) shows that advection of sediment in the water column causes erosion on the south-western side of the basin, while sediment deposition occurs in the northern part and at the end of the basin. Sediment transported by diffusion (Fig. 9(c)) is deposited in small areas near the seaward and landward boundary, whilst in the rest of the basin erosion takes place. The combined effect shown in Fig. 8(c) can, therefore, be interpreted as being largely determined by diffusive fluxes, although advective fluxes are not negligible. When the Coriolis parameter is increased to represent 52° North, the mean advective sediment flux in the landward direction (Fig. 9(b)) experiences a stronger decrease than the diffusive mean sediment flux (Fig. 9(d)) in that direction. This causes the region of dominance of the diffusive mean sediment flux to extend, leading to an enlargement of the erosion area. Finally, we remark that the pattern of the mean advective sediment flux and that of the mean flow field are clearly different. This implies that the mean advective sediment flux is largely determined by correlations between the fluctuating (rather than by the steady) components in velocity and concentration fields. In other words, the mean advective flux is determined by tidal asymmetry rather than by residual currents.

4.3. The progressive tidal wave

The effect of a progressive tidal wave travelling from south to north is again investigated, now with an amplitude of 0.5 m and a time lag over the open boundary of 1500 s. This is done in order to reduce the dominating effect of the progressive Kelvin wave on the mean flow field found in the previous experiments. Fig. 10 shows the results for

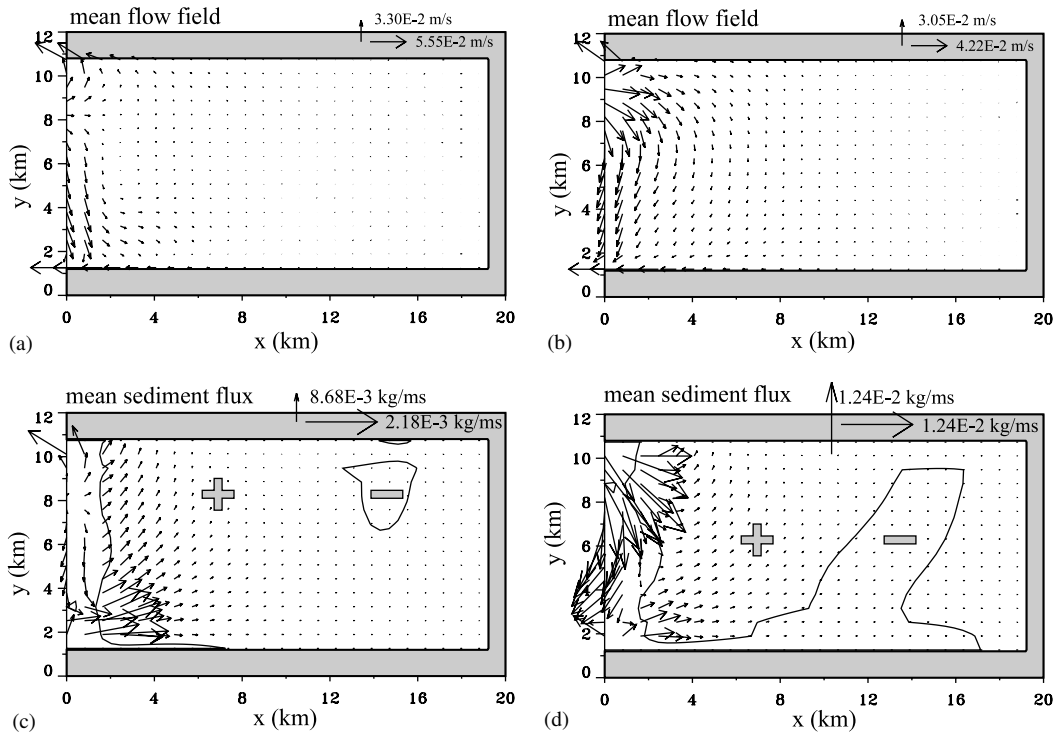

Fig. 10. Mean flow field (above) and mean sediment flux field (below) for: (a, c) only a progressive tidal wave; (b, d) progressive tidal wave with Coriolis effects (52° North). The drawn line is zero convergence of sediment flux, the grey signs indicate deposition (plus) and erosion (minus) areas. The values indicate maximum sediment transport in each direction. Dark grey area is land.

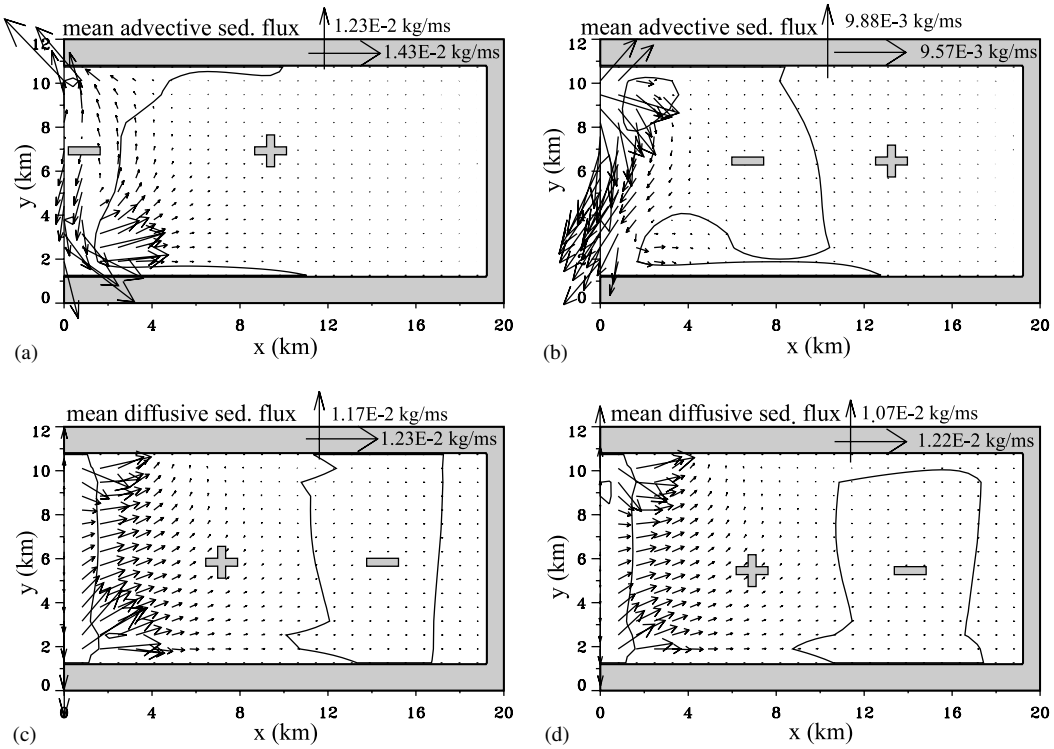

Fig. 11. Mean advective sediment flux field (top) and mean diffusive sediment flux field (bottom) for default settings: (a, c) progressive wave ($\Delta t = 1500$ s); (b, d) Coriolis force (52° North) and progressive wave ($\Delta t = 1500$ s). The drawn line is zero convergence of the plotted sediment flux, the grey signs indicate deposition (plus) and erosion (minus) areas.

the mean flow and mean sediment flux in case of a progressive tidal wave for two cases: no Coriolis effects (Figs. 10(a) and (c)) and with Coriolis effects (52° North, Figs. 10(b) and (d)).

The flow field is in both cases characterised by an inflow point on the northern side of the entrance, with northern and southern deflection. Maximum velocity values are increased by a factor of 10 compared to those obtained with only Coriolis effects (Fig. 8(b)). Including both earth rotation effects and a progressive tidal wave results in a northward shift of the point of inflow and smaller maximum velocities (Fig. 10(b)). Again, the imposed boundary condition of constant water-level amplitude at the open boundary is not natural: in Fig. 6(c) a strong mean water-level gradient was found across the inlet. Therefore, the boundary condition at the entrance will affect the mean flow field near the inlet. The results can, therefore, be interpreted as being representative for the situation with a source of vorticity outside the basin during flood.

The mean sediment flux field in Fig. 10(c) is convergent in large parts of the embayment, indicating the formation of shoals in these areas. If also earth rotation is incorporated, then the effects of both the progressive tidal wave and earth rotation on the erosion-deposition pattern (see Fig. 10(d)) can be recognised. Compared to Fig. 10(c) the area of erosion has clearly extended, in particular towards the southern part of the embayment. Fig. 11 shows the separate effects of the advective and diffusive mean sediment flux for the two cases.

From this it can be seen that in case of no Coriolis effects the net erosion-deposition pattern (see Fig. 10(c)) is determined by diffusive and advective contributions which have a similar

magnitude. Including earth rotation effects causes the advective mean sediment flux to decrease and the basin becomes more diffusively dominated.

Note that in case of a progressive tidal wave the pattern of the mean advective sediment transport resembles that of the mean flow field. This means that the mean advective fluxes are now largely determined by the residual current (rather than by tidal asymmetry).

5. Conclusions and discussion

The experiments with the numerical model have indicated that for tidal basins, resembling those located in the western part of the Wadden Sea, the asymmetry in the flow field can be mostly attributed to phase differences of the large-scale tidal wave along the coast, rather than to the direct effect of earth rotation. Residual circulation cells were found which depend on the prescribed boundary conditions at open sea. In the present experiments (no lateral slopes in the bottom topography) residual circulation cells were found to be mainly caused by advection of tidal vorticity by tidal currents, generated by velocity shear due to sidewall friction. Vorticity production due to Coriolis torques and bottom frictional torques appears to play only a minor role. In case of no Coriolis effects and a standing tidal wave the main source of vorticity is the lateral shear of the along-channel velocity component. However, with earth rotation included and a progressive tidal wave the cross-shore shear of the shore-parallel tidal current is the main source of vorticity production.

The mean sea level patterns were also analysed. It was found that with increasing phase differences of the tidal wave over the open sea boundary an increase of the mean set-up in the basin occurs. Near the seaward entrance it also causes an increase of the cross-channel sea surface gradient with a large set-down at the southern tip.

Analysis of the tidal velocity field revealed no presence of an overshoot of the flood current entering the basin. Stronger tidal ellipticity on the northern part of the outer delta was found only in a very small region attached to the northern headland. The conceptual model of Sha (1989) is, therefore, only partly supported by these experiments. The field data results for the Marsdiep inlet system (Fig. 1(a)), in particular the large area with elliptical tidal currents, are expected to be caused by two effects. One is the geometry of the basin: its length is much larger than that of the basins considered in this study, resulting in different tidal characteristics. The second is the complex morphology of the outer delta of the Marsdiep, in particular the presence of the large sandy shoal 'Noorder Haaks'. Future experiments with the model will include more realistic outer area topography (shoal, channel, slope) to check this hypothesis.

With regard to sediment transport and morphology, the present intermediate model only partly confirms the results previously obtained with idealised morphodynamic models. In particular, it was found that in case of a sloping bed, bottom frictional forces cannot be neglected in the momentum balance, as is done in the idealised model. Nevertheless, the present model is a convenient tool to study the influences of additional physical processes which cannot be easily realised in the idealised model. Here, the role of earth rotation and a progressive tidal wave following the coast were investigated in this respect. It turned out that both the Coriolis force and the tidal wave characteristics cause significant and different patterns of sediment erosion and deposition. An interesting result is that, in the studied short embayment (its length being much smaller than the tidal wavelength) the mean sediment flux caused by the joint effect of earth rotation and a progressive tidal wave is diffusively dominated. With decreasing influence of the Coriolis force advective fluxes become more important and the latter appear to be mainly determined by the steady components of the velocity and sediment concentration. On the contrary, advective fluxes in case of a standing tidal wave are controlled by the fluctuating components of velocity and concentration.

Results of the present model indicate that it is a helpful tool to gain further understanding about the hydrodynamic and morphodynamic processes in tidal inlet systems. In this sense it serves as a link between quasi-realistic models, conceptual models

and idealised models. However, its application is as yet limited because a number of processes are not accounted for. The effect of waves plays an important role on the outer delta (Sha, 1989). Drying and flooding of shoals (hypsometric effects, see Friedrichs and Aubrey, 1994) have to be properly accounted for. In this respect the work of Delfina (2000) offers a possible solution. Also a more sophisticated sediment transport formulation is necessary. In the case of a rectangular basin without outer delta the water level at the entrance is not adjusted for loss of amplitude due to bottom friction or cross-inlet gradients. This obvious lack should be corrected by either a different analytical definition of the water level at the entrance or by including an outer delta in the geometry. The latter would involve an extension which cannot be incorporated in the idealised model, hampering comparison with the idealised model results.

Further research will include combined M_2, M_4 forcing, analysis of tidal components contributing to the advective sediment transport and the influence of the outer delta morphology on the tidal motion and mean sediment transport patterns.

Acknowledgements

The authors thank J. Backhaus for providing the HAMSOM code and E. Spee for the software extensions. This research was supported by NWO-grant no. 750-19-707.

Appendix A. Equations for water motion in the HAMSOM model

The HAMSOM-code used in the present paper solves the one-layer version of the shallow water equations

$$\frac{\partial \vec{u}}{\partial t} + (\vec{u}\cdot\vec{\nabla})\vec{u} + f\vec{e}_z \times \vec{u} = -g\vec{\nabla}\zeta - \frac{\vec{\tau}_b}{\rho(H+\zeta)} + A_h\nabla^2\vec{u}, \quad \text{(A.1)}$$

$$\frac{\partial \zeta}{\partial t} + \vec{\nabla}\cdot[(H+\zeta)\vec{u}] = 0. \quad \text{(A.2)}$$

Here $\vec{u} = (u, v)$ is the depth-averaged velocity vector, ζ is the elevation of the free surface with respect to the undisturbed level, H is the undisturbed water depth, t is the time and $\vec{\nabla} = (\partial/\partial x, \partial/\partial y)$. Furthermore, f is the Coriolis parameter, $\vec{e}_z$ is a unity vector in the vertical, g is the acceleration due to gravity, ρ is the water density and A_h is the diffusion coefficient. For the bed shear stress two different formulations are used

$$\vec{\tau}_b = \rho r\vec{u} \quad or \quad \vec{\tau}_b = \rho c_d |\vec{u}|\,\vec{u}. \quad \text{(A.3)}$$

Here r is a linear friction coefficient ($r \sim 10^{-3}\,\mathrm{ms}^{-1}$) and c_d is a drag coefficient, which is assumed to be constant ($c_d \sim 0.002$).

References

Backhaus, J.O., 1983. A semi-implicit scheme for the shallow water equations for application to shelf sea modelling. Continental Shelf Research 2 (4), 243–254.

Cayocca, F., 2001. Long-term morphological modelling of a tidal inlet: the Arcachon Basin, France. Coastal Engineering 42, 115–142.

Delfina, A., 2000. Two-dimensional shallow flow equations for partially dry areas. Water Resources Research 36 (11), 3251–3264.

Dyer, K.R., 1986. Coastal and Estuarine Sediment Dynamics. Wiley, Chichester.

FitzGerald, D.M., 1996. Geomorphic variability and morphologic and sedimentologic controls on tidal inlets. Journal of Coastal Research 23, 47–71.

Friedrichs, C.T., Aubrey, D.G., 1994. Tidal propagation in strongly convergent channels. Journal of Geophysical Research C 99, 3321–3336.

Lanzoni, S., Seminara, G., 1998. On tide propagation in convergent estuaries. Journal of Geophysical Research C 103, 30793–30812.

Oost, A.P., 1995. Dynamics and sedimentary development of the Dutch Wadden Sea with emphasis on the Frisian Inlet. Ph.D. Thesis, Geologica Ultraiectina, 126, Faculty of Earth Sciences, Utrecht University.

Ridderinkhof, H., 1988. Tidal and residual flows in the western Dutch Wadden Sea 1: numerical model results. Netherlands Journal of Sea Research 22, 1–22.

Ridderinkhof, H., Zimmerman, J.T.F., 1992. Chaotic stirring in a tidal system. Science 258, 1107–1111.

Schuttelaars, H.M., De Swart, H.E., 1996. An idealized long-term morphodynamic model of a tidal embayment. European Journal of Mechanics, B/Fluids 15 (1), 55–80.

Schuttelaars, H.M., De Swart, H.E., 1999. Initial formation of channels and shoals in a short tidal embayment. Journal of Fluid Mechanics 386, 15–42.

Sha, L.P., 1989. Sand transport patterns in the ebb tidal delta off Texel inlet, Wad-den Sea, the Netherlands. Marine Geology 86, 137–154.

Van de Kreeke, J., Robaczewska, K., 1993. Tide-induced residual transport of coarse sediment; application to the Ems estuary. Netherlands Journal of Sea Research 31 (3), 209–220.

Van der Molen, J., 2000. A 2DH numerical model of tidally induced sand transport in the southern North Sea. In: Yanagi, T. (Ed.), Interactions between Estuaries, Coastal Seas and Shelf Seas. Terra Scientific Publishing Company, Tokyo.

Van Leeuwen, S.M., Schuttelaars, H.M., De Swart, H.E., 2000. Tidal and morphologic properties of embayments: effect of sediment deposition processes and length variation. Physics and Chemistry of the Earth 25 (4), 365–368.

Van Rijn, L.C., 1993. Principles of sediment transport in rivers, estuaries and coastal seas. Aqua Publications, Amsterdam.

Wang, Z.B., Louters, T., De Vriend, H.J., 1995. Morphodynamic modelling for a tidal inlet in the Wadden sea. Marine Geology 126, 289–300.

Zimmerman, J.T.F., 1981. Dynamics, diffusion and geomorphological significance of tidal residual eddies. Nature 290, 549–555.